Provided for non-commercial research and education use.
Not for reproduction, distribution or commercial use.

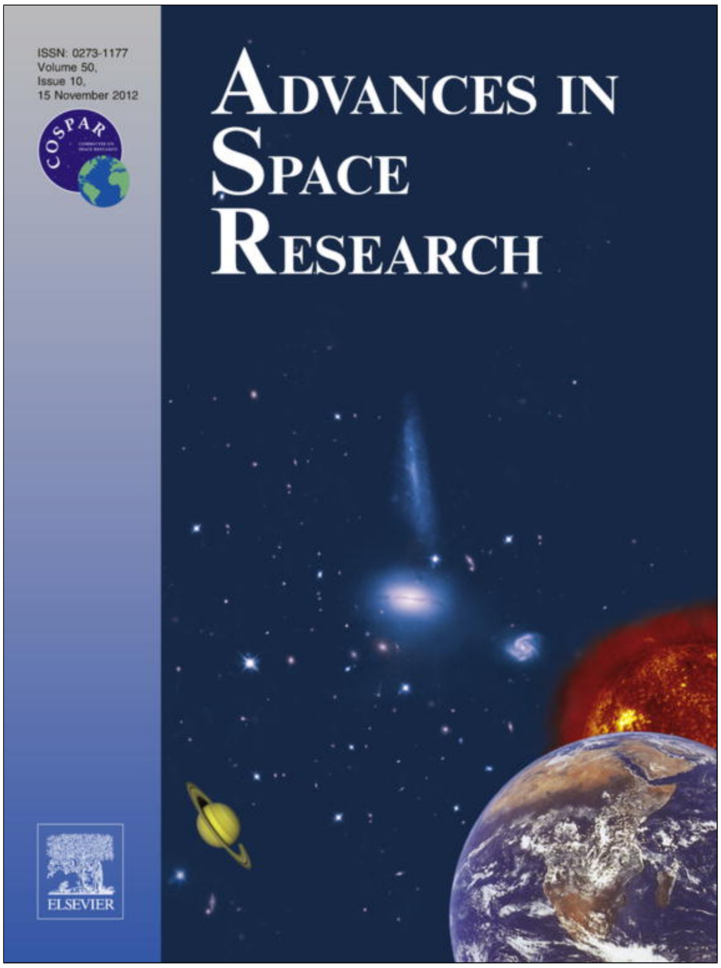

This article appeared in a journal published by Elsevier. The attached copy is furnished to the author for internal non-commercial research and education use, including for instruction at the authors institution and sharing with colleagues.

Other uses, including reproduction and distribution, or selling or licensing copies, or posting to personal, institutional or third party websites are prohibited.

In most cases authors are permitted to post their version of the article (e.g. in Word or Tex form) to their personal website or institutional repository. Authors requiring further information regarding Elsevier's archiving and manuscript policies are encouraged to visit:

http://www.elsevier.com/copyright

Available online at www.sciencedirect.com
SciVerse ScienceDirect
Advances in Space Research 50 (2012) 1411–1424
ADVANCES IN SPACE RESEARCH
(a COSPAR publication)
www.elsevier.com/locate/asr

Degradation of thermal control materials under a simulated radiative space environment

A.K. Sharma *, N. Sridhara

Thermal Systems Group, ISRO Satellite Centre, Vimanapura Post, Bangalore 560 017, India

Received 29 September 2011; received in revised form 7 July 2012; accepted 15 July 2012
Available online 20 July 2012

Abstract

A spacecraft with a passive thermal control system utilizes various thermal control materials to maintain temperatures within safe operating limits. Materials used for spacecraft applications are exposed to harsh space environments such as ultraviolet (UV) and particle (electron, proton) irradiation and atomic oxygen (AO), undergo physical damage and thermal degradation, which must be considered for spacecraft thermal design optimization and cost effectiveness. This paper describes the effect of synergistic radiation on some of the important thermal control materials to verify the assumptions of beginning-of-life (BOL) and end-of-life (EOL) properties. Studies on the degradation in the optical properties (solar absorptance and infrared emittance) of some important thermal control materials exposed to simulated radiative geostationary space environment are discussed. The current studies are purely related to the influence of radiation on the degradation of the materials; other environmental aspects (e.g., thermal cycling) are not discussed. The thermal control materials investigated herein include different kind of second-surface mirrors, white anodizing, white paints, black paints, multilayer insulation materials, varnish coated aluminized polyimide, germanium coated polyimide, polyether ether ketone (PEEK) and poly tetra fluoro ethylene (PTFE). For this purpose, a test in the constant vacuum was performed reproducing a three year radiative space environment exposure, including ultraviolet and charged particle effects on North/South panels of a geostationary three-axis stabilized spacecraft. Reflectance spectra were measured in situ in the solar range (250–2500 nm) and the corresponding solar absorptance values were calculated. The test methodology and the degradations of the materials are discussed. The most important degradations among the low solar absorptance materials were found in the white paints whereas the rigid optical solar reflectors remained quite stable. Among the high solar absorptance elements, as such the change in the solar absorptance was very low, in particular the germanium coated polyimide was found highly stable.

© 2012 COSPAR. Published by Elsevier Ltd. All rights reserved.

Keywords: Thermal control materials degradation; Solar radiation simulation; Geostationary earth orbit (GEO) simulation; Ultraviolet and particle irradiation

1. Introduction

A spacecraft operates in a harsh environment. One side directly faces the sun, while the other side faces deep, cold space (temperature ~4 K). This inflicts large thermal gradient between the sunlit and shadowed sides. The various subsystems of spacecraft, however, operate at the maximum efficiency within a small temperature range. Outside this range, either their efficiency decreases or their lifetime is reduced, and under certain conditions they may stop functioning altogether. As an example, consider Ni–Cd batteries: at temperatures below 273 K, satisfactory operation cannot be achieved, due to poor recombination kinetics of the parasitic reaction products resulting in mechanical damage to the cell; above 313 K, their performance degrades due to inefficient recharging (Sharma, 2005).

On earth, equipment with a tendency to run too cold or too hot may be readily brought back to acceptable operating temperature through heat exchange with the atmosphere. In space, heat exchange is restricted to radiation,

---

* Corresponding author. Tel.: +91 8025205273, 8025083767, 8025083201; fax: +91 8025083203.
E-mail address: aks@isac.gov.in (A.K. Sharma).

0273-1177/$36.00 © 2012 COSPAR. Published by Elsevier Ltd. All rights reserved.
http://dx.doi.org/10.1016/j.asr.2012.07.010

which is a poor substitute for convection. Under these circumstances, the challenge in spacecraft thermal design is to achieve the proper in-orbit operational temperatures for different components of spacecraft.

1.1. Thermal design of spacecraft

If we consider a spacecraft far away from earth's atmosphere and assume that it does not have any internal power dissipation, the steady state temperature of spacecraft can be expressed by the following energy balance equation (Agarwal, 1986):

$$SA_{\mathrm{p}}\alpha = \sigma\varepsilon A T^4$$

$$T = \left[\frac{SA_{\mathrm{p}}\alpha}{\sigma A\varepsilon}\right]^{1/4} \tag{1}$$

where T is the absolute temperature of the spacecraft, K; S is the solar constant (yearly average value at earth is 1366 W m^{-2}); σ is the Stefan–Boltzmann constant (56.7×10^{-9} W m^{-2} K^{-4}); A_p is the projected surface area of the spacecraft perpendicular to solar rays, m^2; A is the total surface area of the spacecraft, m^2; α is the solar absorptance; ε is the thermal emittance of the exposed surface. Because S, σ, A_{p} and A are constants in this relationship, it can be seen that the temperature of a given area of the spacecraft is directly controlled by the α/ε ratio.

Thermal control techniques are broadly grouped into passive and active. Passive thermal control techniques are preferentially adopted for the thermal control of spacecraft. The passive system does not involve any relative movement of its parts and does not require external power for operation. This eliminates the possibility of its failure. The passive thermal control system utilizes coatings, multilayer insulation (MLI) and radiators of known optical properties to achieve the required thermal control. Active thermal control systems require external power for their operations and involve the moving parts, for example- electrical heaters, mechanical refrigerators, thermostatic louvers, pumped fluid loops, electro-optical coatings, etc. The passive thermal control methods are used when simplicity, cost and reliability are the key design factors (Gilmore, 2002; Anvari et al., 2009).

The temperature of spacecraft and its sub systems depends on the internally generated heat of spacecraft, heat absorbed from the sun, and the heat radiated out to space. Thermal control of spacecraft is mainly achieved by isolating it from the harsh environment with the multilayer insulation. The multilayer insulation not only prevents entering the heat from the sun to the spacecraft, but also restricts the rejection of internal generated heat from the spacecraft. Therefore the area where high heat is generated must be exposed to space to allow radiation of excess heat. These areas are called radiators. The satellite radiator presents the interface of the satellite with the outer space, and radiatively couples it to the space environment. To maximize heat rejection and limit heat absorption from the surroundings, radiators operating in the presence of solar energy are characterized by having the combined properties of low solar absorptance and high infrared emittance (low α_s/ε ratio). One of the efficient example of radiator is called optical windows where optical solar reflectors (OSRs) are bonded. OSRs allow rejection of the internally generated heat in the spacecraft to the outer space while reflecting most of the incident solar energy. In addition, thermal control of various subsystems of spacecraft is achieved by the application of various coatings with known optical properties. For example, high emittance coatings are applied on most of the internal components of spacecraft to improve their heat radiation characteristics; similarly, in some other areas, low emittance coating is employed for minimizing the radiative coupling. Further, the coatings used for spacecraft application must be easy to apply, should have low outgassing and stability in space environment.

1.2. Material for spacecraft application

Mass reduction is an important criterion in the spacecraft design, because the cost of a spacecraft launch is enormous. Reduction in structural mass leads to higher payload capability and/or higher fuel mass, resulting in longer spacecraft life. The materials/ coatings used in space technology requires higher standards and better control than those used for ground applications, because an on-orbit spacecraft is not approachable for repair, and space conditions are very severe. The materials designed for space missions have to withstand extreme aerodynamic heating, acceleration, shock, vibration and acoustic noise during space flight, and ultrahigh vacuum, extreme temperature cycling, bombardment by high energy particles (electrons and protons) and extreme temperature cycling in orbit. Solar absorptance is an important parameter of thermal control elements. Increase in the temperature of the spacecraft at the end of long term mission is mainly caused by the degradation of solar absorptance of the thermal control materials under space environment. The extreme conditions in the space environment and the high cost associated with placing the satellites in the orbit require that the satellite materials be thoroughly tested prior to deployment in their respective orbits (Marco et al., 2003, 2009). The application of defective material not only seriously affects the performance of a particular subsystem but also increases the probability of the failure of the entire mission by damaging it permanently. In the present paper degradation of thermal control materials under a simulated radiative space environment is investigated. The current studies are purely related to the influence of radiation on the materials; other environmental aspects (e.g., thermal cycling) are not discussed.

2. Test description

The space environment simulation was carried out at ONERA's SEMIRAMIS combined radiation test facility.

ONERA is a French aerospace research centre, of which the abbreviation stands for: Office National d'Etudes et Recherches Aérospatiales. A long term test extending to over three months in vacuum was performed to simulate a three years radiation exposure on the North-South panels of a 3-axis stabilized geostationary spacecraft. Reflectance spectra were measured in-situ in the solar range (250–2500 nm) and the solar absorptance values were deduced from it. The degradation has been observed most in the white paints while the second surface mirrors have been quite stable. To complete the thermo-optical properties investigations, infrared emissivity measurements were performed in air at the beginning and at the end of the test. The measured values showed good stability, except in the case of conductive black paint and fluorinated ethylene propylene (FEP) based flexible OSR without indium tin oxide (ITO) coating.

2.1. SEMIRAMIS facility

The SEMIRAMIS facility is used to reproduce combined space environment composed of UV, electrons and protons. It's most important capability is to measure in-situ spectral reflectivity of the materials under vacuum avoiding the quick and important bleaching effects that frequently occur when irradiated materials are exposed to the air. Furthermore, the effects of the initial air to vacuum and final vacuum to air transitions can be studied for every test.

The SEMIRAMIS test facility is composed of two parts. At the lower stage, there is an irradiation chamber with three ports, one for protons at the normal of the samples, one for electrons and UV at 30° of incidence and one for a multipurpose accessory housed in a lateral vacuum chamber (cryogenic trap or Knudsen contamination cells or a radiant sample temperature measurement system).

At the upper stage, there is a measurement and safeguard chamber in which the sample holder can be introduced by a vertical translation from the lower stage and connected to an optical measurement device stored in an another lateral vacuum chamber. The in-situ measurement system is composed of a spectrophotometer which is connected to a mobile integrating sphere in vacuum. Reflectance spectra (250–2500 nm) of about 25 samples can be measured without breaking vacuum between the irradiation phases.

2.2. Samples description: samples position and measurement points

Totally 20 samples were subjected for the evaluation. 18 Samples were supplied by the ISRO, while two additional samples of evaporated aluminium were used as reference specimen (1 irradiated and 1 non-irradiated). All these samples were bonded on aluminium plate for the irradiation test. The details of the test samples are presented in Table 1. As the in-situ measurement system is adapted for reflectance measurements, all the samples were opaque (except PEEK and white paint) and equipped with a reflective rear face. PEEK is primarily investigated for its physical degradation and the degradation of its solar abrorptance is only an indicative parameter. White paints with different back-ups were investigated to evaluate their effective solar absorptance degradation in the different application conditions. There were 21 measurement points in the irradiated area on the 19 samples. Measurements on two OSR samples were made at two diagonal positions due to their larger size (40 × 40 mm) and results shown are the maximum value of the two measurements. While the measurements on all other samples (19.8 × 19.8 mm) were made only at one centre point. A photograph of test sample holder is shown in Fig. 1.

2.3. Vacuum and contamination control

Solar absorptance is very sensitive to the surface contamination. The test setup had several methods to control the sample contamination such as low contamination vacuum system, cryogenic shroud and the higher sample temperature.

After the initial out gassing period of 2.5 days at 333 K, 3.8×10^{-7} mbar pressure was attained and it was maintained at 10^{-7} mbar during the entire test. The residual contamination level is measured during the test at the ambient temperature with a Quartz Crystal Microbalance (QCM Maxtek TM300 of a sensitivity of about 3 Å/Hz for density of 1) set at the bottom of the irradiation chamber. Though the QCM was not directly irradiated, frequency measurement was modified by the UV presence. The variation in the two conditions with or without UV was about 20 Hz during the test. It corresponds to a very low level contamination of about 60 Å.

2.4. Temperature control

Temperature of samples was controlled by providing good thermal contact with sample holder and connecting it to a constant temperature water circulation unit. The sample holder is composed of two parts, a front sample holder aluminium plate and a rear part where water circulation is used. The test samples were fixed over aluminium plate (19.8 × 19.8 mm for 17 samples and 42 × 42 mm for 2 samples) and mounted on the sample holder with screwed metallic strips as shown in Fig. 1. The temperature of the front part was maintained at 333 K during the UV test and 336 K during measurements and particle irradiation test.

2.5. UV irradiations

Bi-Lambda 4 ultraviolet generator equipped with 6500 Watts Xenon sources whose spectral distribution in the UV is close to that of the sun was used. The source emission was filtered rejecting all visible and infrared light above 400 nm, in order to reproduce only the sun UV outer

Table 1
Details of irradiated samples.

Sl. no.	Description	Remarks
1	Rigid OSR 1(GOAL)	40 × 40 × 0.2 mm
2	Rigid OSR 2 (QiOptiq)	40 × 40 × 0.08 mm
3	Flexible OSR (ISRO, Without ITO coating)	FEP/Ta_2O_5/Ag/Inconel; 125 μm
4	Flexible OSR (Sheldahl, with ITO coating)	ITO/FEP/Ag/Inconel; 125 μm
5	MLI Blanket	ITO coated polyimide aluminized rear side (Sheldahl, 50 μm) + polyester net (Haren Textile, 175 μm) + aluminized polyester (Pan Electronics, 6.25 μm) + Polyester Net (Harren Textile, 175 μm) + ITO coated aluminized polyimide (Sheldahl, 50 μm)
6	Germanium coated polyimide (ISRO)	Ge coated on 25 μm black polyimide
7	ITO coated aluminized polyimide (ISRO)	50 μm
8	PEEK	0.5 mm sheet
9	PTFE	0.5 mm sheet
10	Conductive black paint (Aeroglaze Z307, Lord Corp.)	75 μm paint on Al
11	White paint-1 (SG121FD, MAP)	70 μm SG121FD paint on 25 μm polyimide
12	White paint-2 (SG121FD, MAP on polyimide + Aeroglaze Z306, Lord Corp. on the rear side)	70 μm SG121FD paint on 25 μm polyimide; 20 μm Aeroglaze Z306 on the rear side.
13	White paint-3 (Chemiglaze Z202 Flexwhite, Lord Corp.) on polyimide	70 μm Chemiglaze Z202 on 25 μm polyimide
14	White Paint-4 (Chemiglaze Z202 Flexwhite, Lord Corp. on polyimide + Aeroglaze Z306, Lord Corp. on the rear side)	70 μm Chemiglaze Z 202 Flexwhite paint on 25 μm polyimide; 20 μm Aeroglaze Z306 on the rear side
15	White paint-5 (Chemiglaze Z202 Flexwhite, Lord Corp. + Aeroglaze Z306, Lord Corp. on polyimide)	70 μm Chemiglaze Z 202 Flexwhite paint + 20 μm Aeroglaze Z306 on 25 μm polyimide
16	White anodized AA 2024 (ISRO)	12.5 μm thickness, Modified Reynolds process (Wernick and Pinner, 1972)
17	Polyimide aluminized (ISRO)	25 μm
18	Varnish coated Aluminized Polyimide (MAP)	100 μm MAPSIL QS1123 varnish on 25 μm Aluminized polyimide. MAPSIL is a 2 component silicone elastomer, base and curing agent ratio 10:1.
19	Reference Material: evaporated aluminum (MTO)	Aluminum on glass protected with SiO_2 coating

Except Sl No. 1 & 2 all samples are of 19.8 × 19.8 (±0.1) mm size. All samples are bonded over aluminum plate. Total thickness of bonded test sample and aluminium plate is 4+0/−0.1 mm.

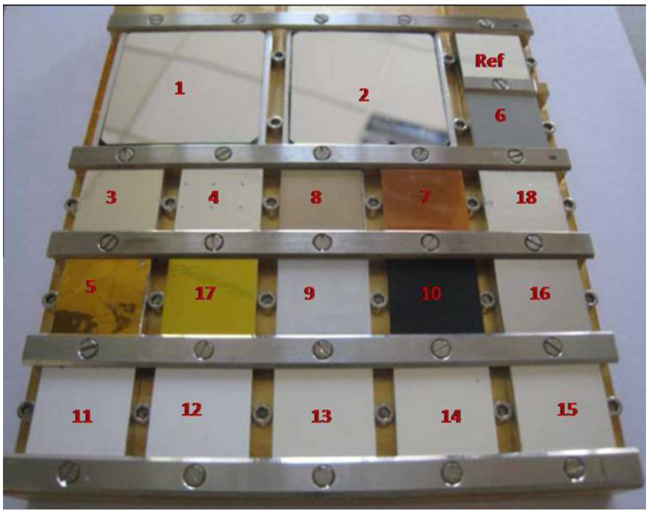

Fig. 1. Photograph of test sample holder.

atmosphere emission (Fig. 2). In space, the solar constant (ASTME 490-00, revised 2006) is 1366 Wm^{-2} (on the complete spectrum from UV to infrared), the corresponding part in the UV range 200-380 nm is 85.7 Wm^{-2}. The filtered source provided the incident power of ~800Wm^{-2} (7 times the UV part of the solar constant, in the range 200-380 nm and the remaining light between 380-450 nm) (Marco et al., 2009).

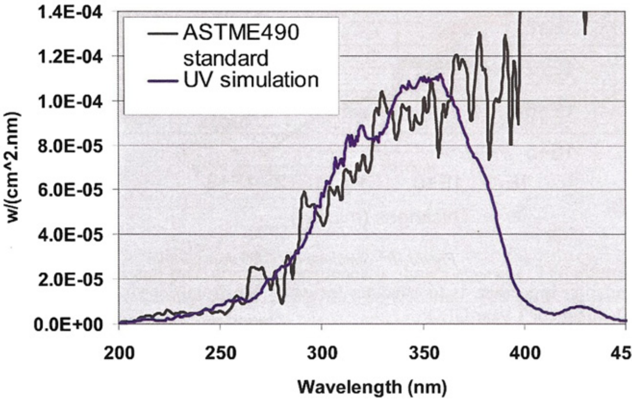

Fig. 2. UV Simulation compared to space.

Two UV lamps were used. The flux was measured/adjusted periodically using a mirror to reflect the flux on a spectroradiometer outside the chamber. The number of laboratory irradiation hours multiplied by the number of used solar constants gives the UV dose in Equivalent Sun Hours (ESH) that is equivalent to the number of hours in space. For 1 year North-South faces of a geostationary spacecraft, it corresponds to 1112 ESH (3336 for the whole test). The total applied dose was little higher than the geostationary earth orbit (GEO) dose as shown in Table 2.

Table 2
UV irradiation dose.

Step	GEO, N/S dose	Applied dose
0.5 year	556 ESH	552 ESH
1 year	1112 ESH	1112 ESH
2 year	2224 ESH	2253 ESH
3 year	3336 ESH	3460 ESH

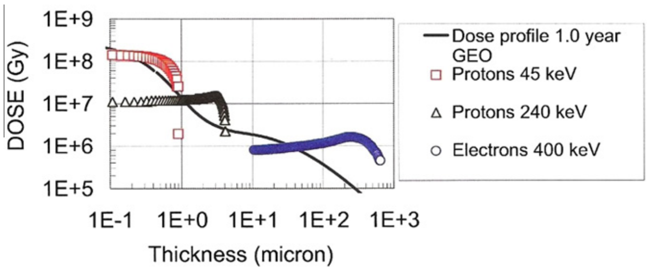

Fig. 3. Simulation of GEO particle dose profile.

2.6. Particle irradiations

In the GEO orbit, the dose profile inside a material, due to the absorption of trapped electrons and protons, decreases rapidly from the surface down to the bulk of the materials. The dose profile was simulated at the laboratory using the addition of the dose profiles of mono-energetic particles. Fig. 3 shows the dose profile calculation (based on trapped particles evaluated with AE8 and AP8 models) inside a material of a typical density of 1.5. On the curve, the protons and electron energies are superimposed in order to fit one year GEO dose profile. In space the dose profile at the surface is mainly due to protons and simulated with two energies of protons 45 and 240 keV, whereas it is due to the electrons in the bulk and simulated with one irradiation of 400 keV energy.

The simulation procedure was to irradiate for each step from the volume up to the surface with the corresponding fluences for 1 year GEO:

- 1×10^{15} electrons cm^{-2} of energy 400 keV at a mean flux of about 5.6×10^{10} electrons cm^{-2} s^{-1} (9 nA cm^{-2}) in order to simulate the space dose in the bulk,

- 2×10^{14} protons cm^{-2} of energy 240 keV at a mean flux of about 1.56×10^{11} protons cm^{-2} s^{-1} (25 nA cm^{-2}) in order to simulate the space dose below the surface.

- 2×10^{15} protons cm^{-2} of energy 45 keV at a mean flux of about 1.56×10^{11} protons cm^{-2} s^{-1} (25 nA cm^{-2}) in order to simulate the space dose close to the surface.

The proton and electron beams were supplied by 2.5 and 2.7 MeV Van de Graaff accelerators, respectively. The protons were obtained from pure hydrogen plasma and separated from the other charged species by a magnetic mass analysis after acceleration. The flux was measured with uniformity of ±15%. The electrons were obtained after diffusion through a thin aluminium window 20 µm thick and measured with uniformity of ±10%. The obtained fluences and fluxes during the test are given in Table 3.

2.7. Test sequence

The 3 years geostationary earth orbit, UV, particles and measurements sequence is shown in Fig. 4. The ultraviolet irradiation was carried out nearly without discontinuity except during flux adjustments. The particles irradiation was done in sequence after the UV irradiations.

2.8. Optical measurements

2.8.1. Spectral reflectance measurements

Spectral measurements were carried out in the range of 250–2500 nm on all the samples and the reference material.

2.8.2. Solar absorptance

The spectral measurements (250–2500 nm) were performed in-situ in the SEMIRAMIS facility. The air initial spectra were calibrated using reflectance spectra performed on another ex-situ spectrophotometer.

Table 3
Applied particles fluencies.

Duration	Particles	Step dose (part/cm^2)	Applied step dose (part/cm^2)	Total dose (part/cm^2)	Applied total dose (part/cm^2)	Flux (nA/cm^2)
0.5 year	Electrons 400 keV	5.00E+14	5.55E+14	5.00E+14	5.55E+14	8
	Protons 240 keV	1.00E+14	1.20E+14	1.00E+14	1.20E+14	26
	Protons 45 keV	1.00E+15	9.64E+14	1.00E+15	9.64E+14	25
1 year	Electrons 400 keV	5.00E+14	4.74E+14	1.00E+15	1.03E+15	8
	Protons 240 keV	1.00E+14	9.17E+13	2.00E+14	2.12E+14	26
	Protons 45 keV	1.00E+15	1.00E+15	2.00E+15	1.96E+15	25.5
2 year	Electrons 400 keV	1.00E+15	9.59E+14	2.00E+15	1.99E+15	8
	Protons 240 keV	2.00E+14	1.86E+14	4.00E+14	3.98E+14	24
	Protons 45 keV	2.00E+15	2.00E+15	4.00E+15	3.96E+15	26
3 year	Electrons 400 keV	1.00E+15	1.01E+15	3.00E+15	3.00E+15	6
	Protons 240 keV	2.00E+14	2.02E+14	6.00E+14	6.00E+14	24
	Protons 45 keV	2.00E+15	2.02E+15	6.00E+15	5.98E+15	24.5

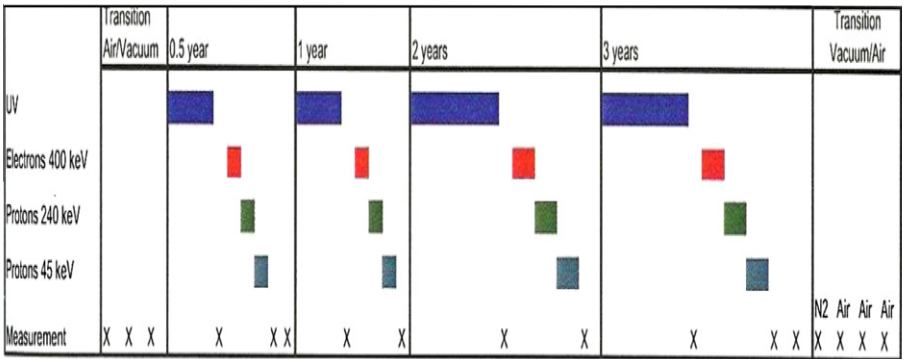

Fig. 4. Three years GEO UV, particles irradiations and measurements sequence.

Calculated solar reflectance is Rs

$$= \frac{\int_{250}^{2500} R(\lambda) \cdot I(\lambda) \cdot d\lambda}{\int_{250}^{2500} I(\lambda) \cdot d\lambda} \qquad (2)$$

where $R(\lambda)$ is spectral reflectance and $I(\lambda)$ is outer atmosphere solar irradiance (defined at 1 AU from the sun).

The solar absorptance, α_s of the reflective samples is deduced from the solar reflectance R_s by using the expression:

$$\alpha_s = 1 - R_s \qquad (3)$$

Relative uncertainty is $\frac{\Delta R_s}{R_s} = \frac{\Delta \alpha_s}{\alpha_s} \approx \pm 1\%$

2.8.3. Normal infrared emissivity

Normal emissivity ε_N is measured in air at the beginning and at the end of the test using an AZ Technology TEMP2000A emissometer.

3. Results and discussion

The main observable degradations are the color changes of the samples, darkening of low absorbing materials and bleaching of the black paint. Some cracks are found on the flexible OSRs and many micro cracks on the varnish.

Solar absorptance values of the samples at various stages and difference in solar absorptance values after UV and particle irradiation ($\Delta\alpha_s$) are presented in Table 4. Final normal emissivity compared to initial values under air is given in Table 5. The emissivity changes for most of the materials are very small, lower than ±0.025. The largest emissivity change of +0.043 is found for the flexible optical solar reflector without ITO (sample 3).

3.1. Overview of samples degradation

An overview of the solar absorptance degradations under vacuum of all the samples is given in Table 4. The general tendency is the saturation of the degradations. The degradations of films and paints occur mainly in the UV and visible range.

3.2. Reference materials

Aluminium evaporated sample was used as a reference material. The stability of the aluminium evaporated references before and after irradiation is verified within ±0.01 uncertainty. The final spectral measurements show a slight degradation and a spectral shift in the UV of the irradiated sample probably due to the formation of more colour centres in the SiO_2 coating. SiO_2 is used as a protective coating over aluminium and it has a negligible effect on the solar absorptance. The reflectance spectrum of the reference sample in vacuum during the test is presented in Fig. 5.

3.3. Optical solar reflectors (OSRs)

Optical solar reflectors are used to reflect the heat generated by the various components of the spacecraft to the outer space. OSRs comprise a thin sheet of glass or quartz (~100 μm), silverized or aluminized on one side by the vacuum evaporation. The solar reflectors are bonded from the silverized side to the desired exterior surface of the spacecraft with a high conduction adhesive. Solar reflectors typically occupy the areas where high heat dissipating equipments are located, e.g., traveling tube wave amplifier and output multiplexer. OSRs perform the dual function of solar reflector and infrared emitter. Optical solar reflectors are also known as second surface mirrors. Because glass is transparent over the solar spectrum, most of the solar radiation reaches the silver coated rear surface and is reflected back (effectively from the second surface) to space. Glass is, however, an excellent emitter over the infrared spectrum, which means that the thermal energy from the spacecraft's interior is conducted via silver to glass and is radiated to outer space.

On the front surface of OSR, transparent conductive coating (TCC) of indium tin oxide (ITO) is applied to prevent the electro static charging on the surface without significantly affecting the thermo-optical properties. During coating the edges are also coated to establish the electrical continuity between the front and rear surface. For low solar absorptance OSRs, stacks of hafnium and silicon dioxide are deposited over the ITO layer. This stack reflects ultraviolet radiation.

Table 4
Solar absorptance values

Sl. no.	Sample	α_S											$\Delta\alpha_s$	
		Air	In Vac 2.5 day	UV 0.5y	Part 0.5y[a]	UV 1y	Part 1y[a]	UV 2y	Part 2y[a]	UV 3y	Part 3y[a]	In air final		
		(1)	(2)	(3)	(4)	(5)	(6)	(7)	(8)	(9)	(10)	(11)	(10)–(2)	(11)–(1)
1	Rigid OSR1	0.034	0.040	0.035	0.038	0.039	0.048	0.039	0.050	0.060	0.050	0.043	0.010	0.009
2	Rigid OSR2	0.026	0.032	0.031	0.033	0.037	0.044	0.042	0.047	0.051	0.050	0.049	0.018	0.023
3	Flexible OSR without ITO	0.110	0.113	0.212	0.180	0.307	0.184	0.211	0.222	0.248	0.253	0.228	0.140	0.118
4	Flexible OSR	0.066	0.061	0.102	0.102	0.109	0.115	0.124	0.145	0.160	0.157	0.134	0.096	0.068
5	MLI blanket	0.365	0.357	0.355	0.402	0.398	0.433	0.421	0.488	0.473	0.528	0.462	0.171	0.097
6	Germanium coated polyimide	0.625	0.621	0.618	0.617	0.620	0.622	0.620	0.618	0.616	0.624	0.624	0.003	(−)0.001
7	ITO coated aluminized polyimide	0.419	0.418	0.434	0.455	0.456	0.480	0.474	0.522	0.511	0.559	0.505	0.141	0.086
8	PEEK	0.441	0.498	0.551	0.575	0.592	0.602	0.603	0.631	0.628	0.650	0.606	0.152	0.165
9	PTFE	0.300	0.275	0.356	0.368	0.405	0.415	0.413	0.452	0.465	0.492	0.445	0.217	0.145
10	Conductive black paint	0.966	0.966	0.955	0.954	0.954	0.952	0.950	0.949	0.948	0.947	0.948	(−)0.019	(−)0.018
11	White paint -1	0.248	0.245	0.253	0.282	0.309	0.333	0.327	0.406	0.394	0.452	0.375	0.207	0.127
12	White paint - 2	0.294	0.286	0.293	0.323	0.349	0.374	0.373	0.445	0.443	0.488	0.429	0.202	0.135
13	White paint - 3	0.262	0.251	0.492	0.504	0.579	0.595	0.623	0.664	0.669	0.694	0.639	0.443	0.377
14	White paint - 4	0.317	0.309	0.532	0.550	0.620	0.635	0.664	0.701	0.708	0.731	0.684	0.422	0.367
15	White paint - 5	0.276	0.265	0.513	0.523	0.596	0.605	0.639	0.671	0.676	0.703	0.658	0.438	0.382
16	White anodized aluminum	0.233	0.246	0.251	0.254	0.264	0.269	0.265	0.270	0.263	0.285	0.290	0.039	0.057
17	Polyimide aluminized	0.332	0.332	0.337	0.370	0.376	0.418	0.422	0.485	0.484	0.527	0.470	0.195	0.138
18	Varnish coated aluminized polyimide	0.134	0.129	0.175	0.195	0.235	0.268	0.298	0.348	0.354	0.398	0.302	0.269	0.168
19	Reference Material: evaporated aluminum	0.098	0.092	0.097	0.090	0.096	0.101	0.094	0.089	0.088	0.108	0.109	0.016	0.011

[a] Electron and proton irradiation.

Table 5
Normal emissivity: initial/final.

Sample no.	Description	Normal emissivity		
		initial	final	Variation (final – initial)
1	Rigid OSR 1	0.861	0.862	0.001
2	Rigid OSR 2	0.875	0.886	0.011
3	Flexible OSR without ITO	0.857	0.900	0.043
4	Flexible OSR with ITO	0.861	0.883	0.022
5	MLI blanket	0.769	0.784	0.015
6	Germanium polyimide	0.905	0.912	0.007
7	ITO coated aluminized polyimide	0.862	0.871	0.009
8	PEEK	0.967	0.970	0.003
9	PTFE	0.974	0.971	−0.003
10	Conductive black paint	0.956	0.932	−0.024
11	White paint-1	0.972	0.973	0.001
12	White paint-2	0.977	0.979	0.002
13	White paint-3	0.955	0.942	−0.013
14	White paint-4	0.963	0.948	−0.015
15	White paint-5	0.965	0.951	−0.014
16	White anodized Aluminum	0.885	0.891	0.006
17	Aluminized Polyimide	0.791	0.813	0.022
18	Varnish Coated Aluminized Polyimide	0.922	0.925	0.003
19	Al. Ref sample	0.050	0.046	−0.004
20	Al. Ref sample (not irradiated)	0.046	0.046	0.000

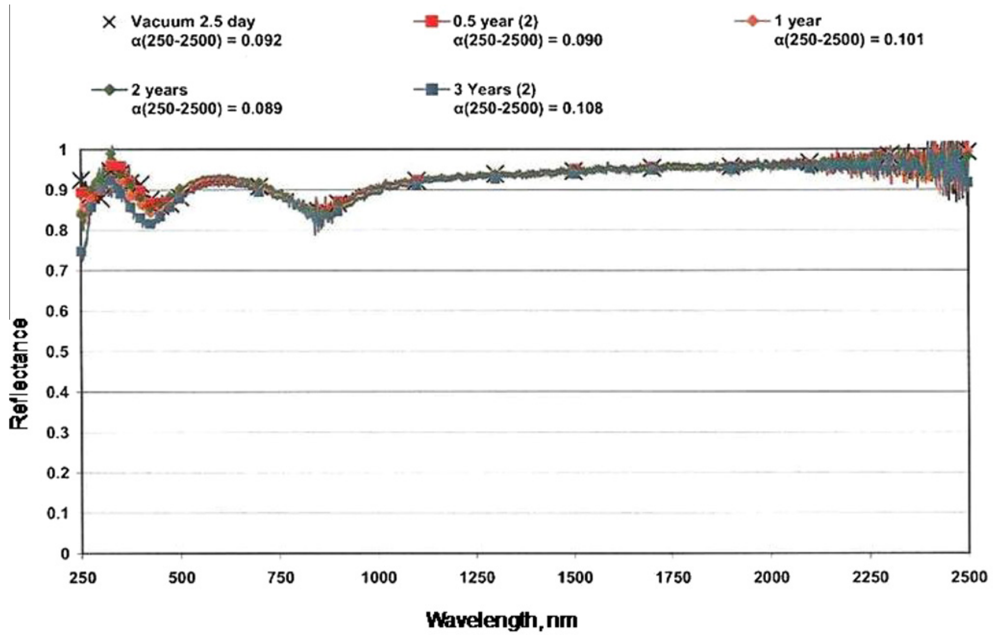

Fig. 5. Reflectance spectrum of the reference sample in vacuum during the test.

Because of rigidity, application of rigid OSR's is limited to only the flat surfaces. As an alternative, flexible OSRs, white paints or white anodizing are used over curved and complex shaped areas. In flexible OSRs, about ~125 μm thick PTFE or FEP film is used in place of quartz substrate. Although rigid solar reflectors cost much more than alternative materials, they are used preferentially because of their improved optical properties and relatively low rate of degradation in space.

Fig. 6 shows the degradation of solar absorptance of OSRs. As expected, the rigid optical solar reflectors show better stability in comparison to the flexible OSR. Further the rigid OSR with a stack of low/high index materials (hafnium and silicon dioxide) for UV reflection show very low degradation ($\Delta\alpha_s$ +0.010, for OSR 1 and +0.018 for OSR 2). Flexible OSR without ITO showed more degradation ($\Delta\alpha_s$ +0.140) than flexible OSR with ITO ($\Delta\alpha_s$ +0.096). The reflectance spectra of rigid and flexible OSR in vacuum

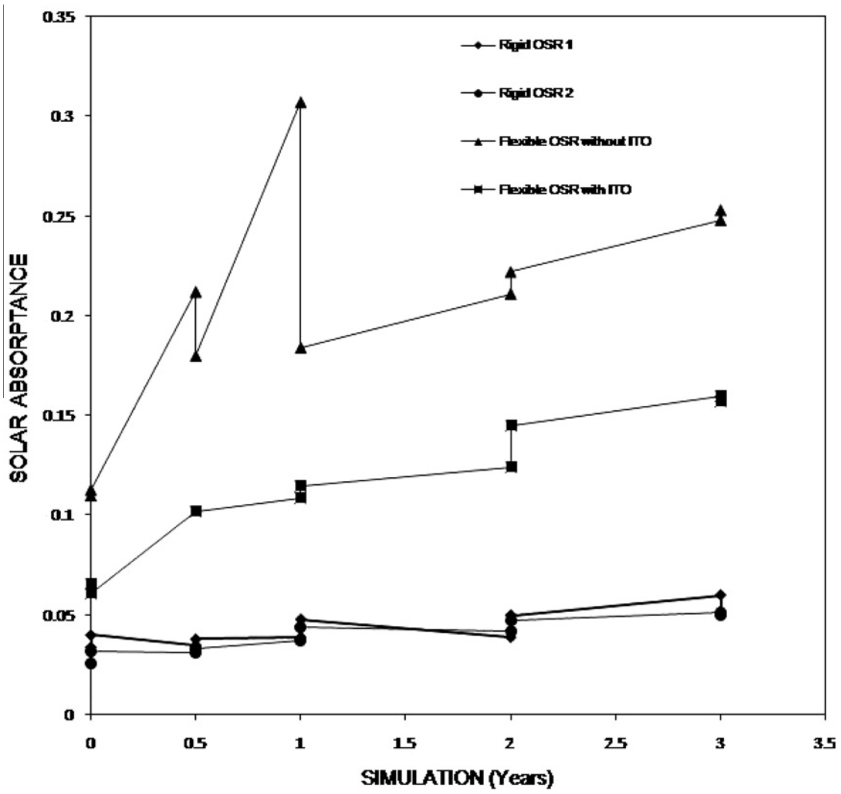

Fig. 6. Solar absorptance degradation of OSRs.

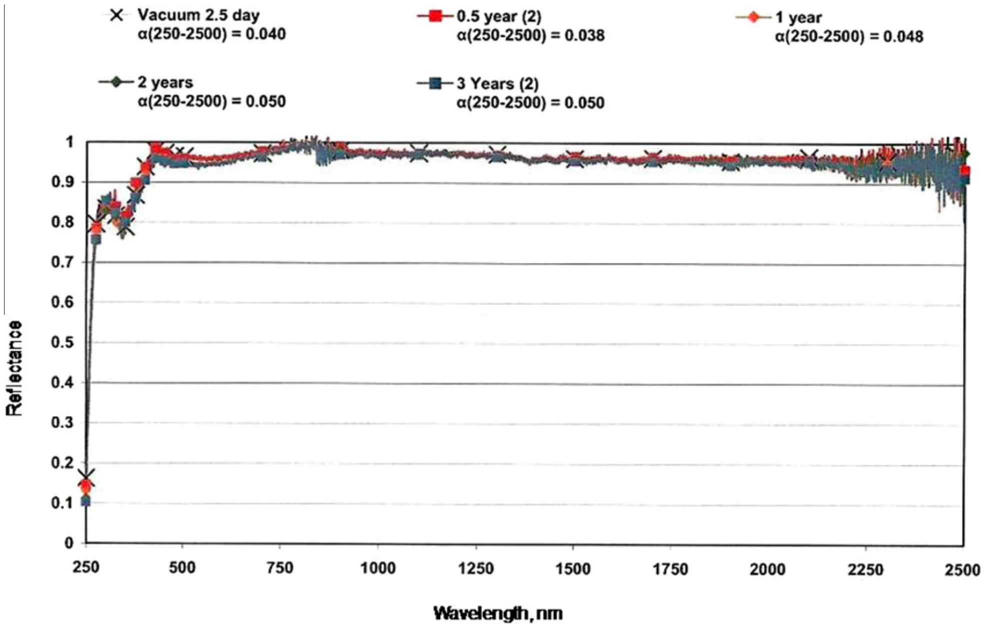

Fig. 7a. Reflectance spectrum of rigid OSR 1 in vacuum during the test.

during the test are shown in Figs. 7 (a & b) and 8 (a & b), respectively.

3.4. Films and polymers

ITO coated aluminized polyimide is used in the fabrication of multilayer insulation blankets. Aluminized polyimide acts as a radiation shield reflecting most of the incident radiation. Transparent conductive ITO coating is used to bleed off the electro static charging. PEEK is as such not used as a thermal control element but as a mechanical supporting material. It retains its mechanical strength in the adverse space condition. The degradation of solar absorptance of PEEK is therefore is of a little importance. Var-

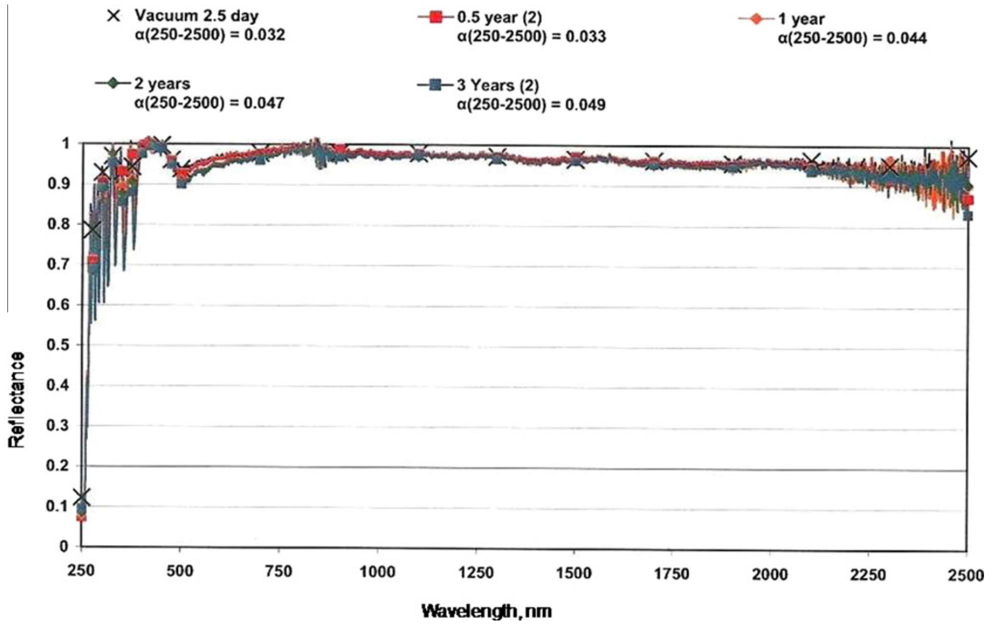

Fig. 7b. Reflectance spectrum of rigid OSR 2 in vacuum during the test.

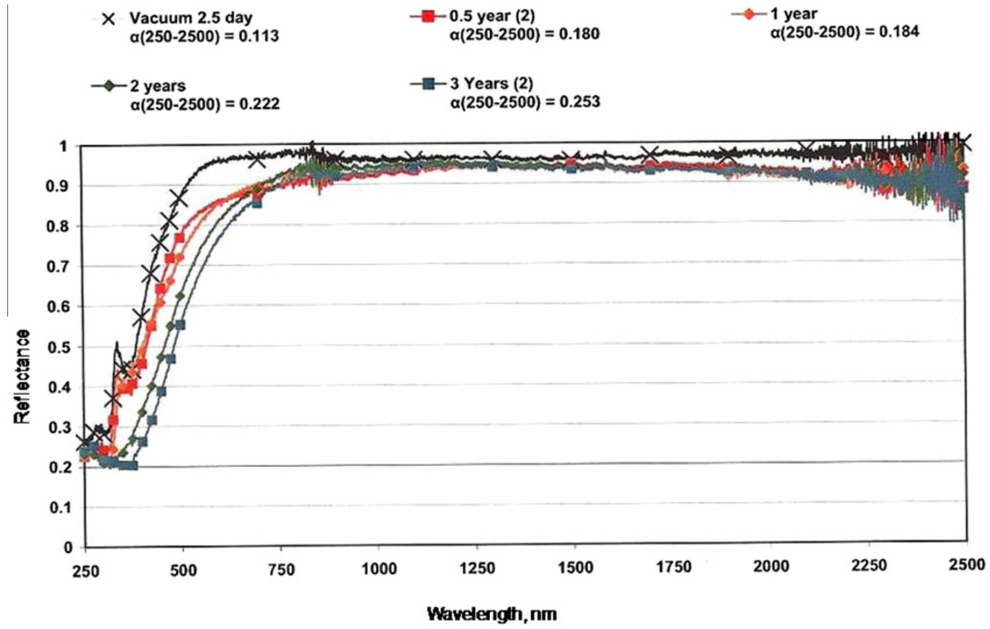

Fig. 8a. Reflectance spectrum of flexible OSR without ITO in vacuum during the test.

nish coated aluminized polyimide is used as a second surface mirror as an alternative to the flexible OSR. It is used to radiate the internally generated heat to the outer space.

Solar absorptance degradation of the films and polymers is shown in Fig. 9. As a general rule the degradation is the highest for the samples having the lowest initial solar absorptance value. PEEK is an exception showing an appreciable degradation despite its initial solar absorptance value is rather higher. The degradation was faster during initial stage of irradiations and it slows down latter. Degradation corresponding to 0.5 year ($\Delta\alpha_S = +0.077$) was about half of the total degradation ($\Delta\alpha_S = +0.152$) in 3 years.

Moderate degradation is observed for the ITO coated aluminized polyimide film. This degradation is mainly due to particle irradiations as can be seen from Table 4. While UV and particles are responsible for the degradations of PTFE and varnish coated aluminized polyimide. Important bleaching is found during final transition to air for these materials. Many micro cracks were observed on the varnish.

Germanium coatings offer several unique features when used in thermal control applications. It provides a surface resistivity of the order of 10^8 Ω/□ for static charge dissipation, an absorptance to emittance ratio of about 0.6, and is

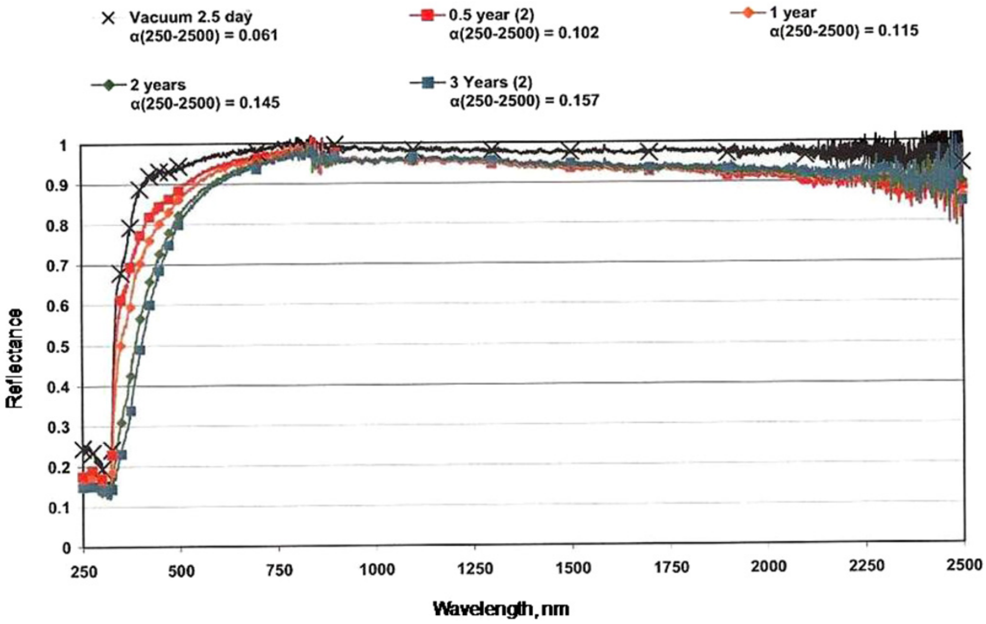

Fig. 8b. Reflectance spectrum of flexible OSR with ITO in vacuum during the test.

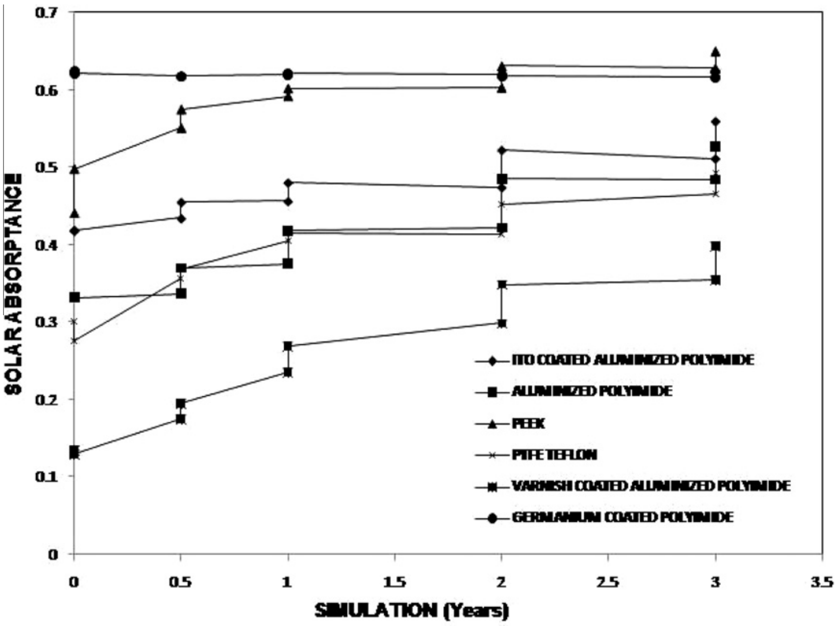

Fig. 9. Solar absorptance degradation of the films and polymers.

transparent to the RF spectrum. Germanium coated polyimide is often used as a sunshield to protect RF antennae from solar radiation. Because germanium is a semiconductor, it is an insulator at radio frequencies. It is largely transparent to the thermal IR, though there can be substantial surface reflection due to its high refractive index. Germanium has some absorption bands near the visible that give raise to a high refractive index and reflection of about 40% of the solar energy. The germanium polyimide film is highly stable with a very low tendency to bleach under irradiations $\Delta\alpha_S \leqslant +0.003$.

3.5. Multilayer insulation

Multilayer insulation consists of alternative layers of heat reflecting radiation shields separated by low conductance spacers. A thin, low emittance radiation shield reflects a large percentage of the radiation it receives from the warmer surface. The spacer reduces the heat transfer from shield to shield by the contact conductance. A conventional multilayer insulation blanket consists of 10–15 alternative layers of aluminized polyester and spacer. Aluminized polyester is a PET (Polyethylene Terephthalate) film of about 6 μm thick, aluminized on both sides, and spacer is polyester net, about 175 μm thick. The top and bottom of these layers are supported by a 25/50 μm thick aluminized polyimide film, which provides the required mechanical strength to the blanket.

The MLI blanket used for irradiation testing is constructed with ITO coated aluminized polyimide/ polyester net/ aluminized polyester/ polyester net / ITO coated aluminized polyimide.

The outer layer, ITO coated aluminized polyimide, in MLI blanket is exposed for the radiation. An increase in the solar absorptance by 0.171of the outer layer of MLI blanket is observed after UV and particle irradiation. The degradations are mainly due to the particles irradiation as expected for aluminized polyimide. A marginal difference in the degradation of the solar absorptance of outer layer of MLI blanket and ITO coated aluminized polyimide may be due to the different source of materials and the processes adopted for the deposition of the outer ITO coating.

3.6. Black paint

Aeroglaze Z306 is an absorptive polyurethane paint. The paint cures to a flat black finish that exhibits a low out gassing characteristics while providing high thermal absorptivity. In the current study, Aeroglaze Z306 is not exposed directly to irradiation. It is used as a base coating, for the fabrication of RF-transparent thermal protection shields (white paint 2, 4 & 5).

Aeroglaze Z307 is polyurethane based electrically conductive black paint. The paint cures to a flat black finish with a low out gassing while providing static dissipation and high thermal absorptivity. In the present study the degradation characteristics of Aeroglaze Z307 are investigated by direct exposer to UV and particles irradiation. The reflectance spectrum of conductive black paint Aeroglaze Z307 in vacuum is presented in Fig. 10. The paint bleaches marginally ($\Delta\alpha_S$ = -0.019) and the half of this variation is observed under the UV for the first 0.5 year step.

3.7. White paints

White paints with low solar absorptance and high thermal emittance characteristics are used as a solar reflector coating to dissipate the internal generated heat in the spacecraft to the outer space. White paints are also used to fabricate the RF-transparent thermal control barrier shields.

SG121FD white paint (Binder: polydiméthylsiloxane, Pigment: treated ZnO, Solvent: Aromatic and aliphatic) provides excellent thermo-optical properties and high resistance to adverse space environment, low Total Mass Loss (TML) and Collected Volatile Condensable Materials (CVCM)% and can withstand very low temperatures, 103 K). Chemiglaze Z202 Flexiwhite is a polyurethane based white paint.

Five different combinations for white paint (1-5) are studied in the present investigation. White paints have some transparency to the solar radiations and a relatively poor adhesion on a polyimide film. To overcome these problems, Aeroglaze Z306 black paint was used as a base coating in different combinations (white paint 2, 4 & 5). This combination is made based on some specific applications, i.e., fabrication of RF transparent thermal protection shield. Here the effective degradation accounts for the combined effect of the white paint and the rear coating material. Solar absorptance degradation of white paints is presented in Fig. 11.

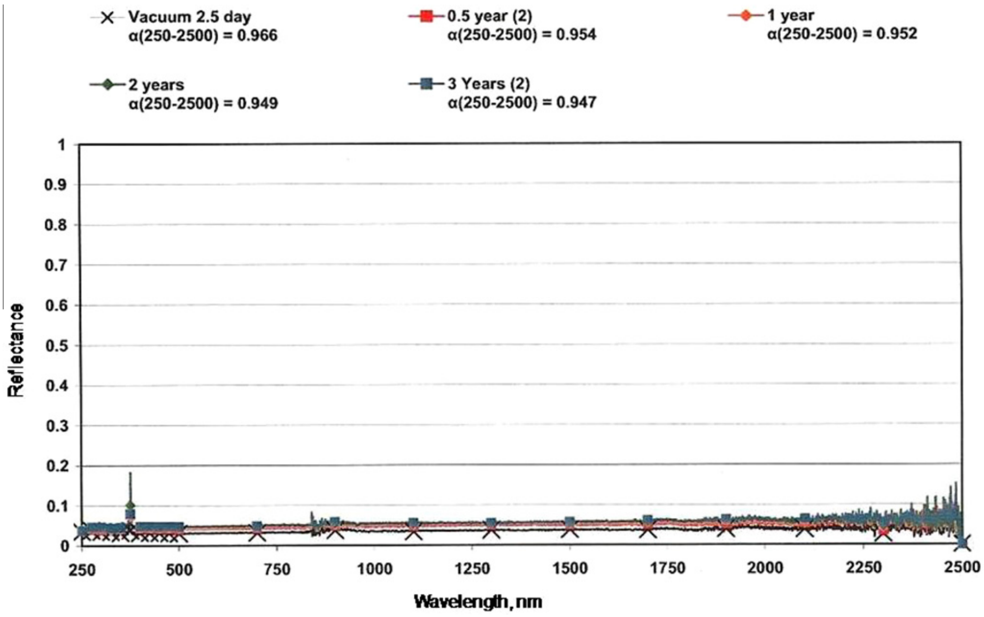

Fig. 10. Reflectance spectrum of conductive black paint in vacuum during the test.

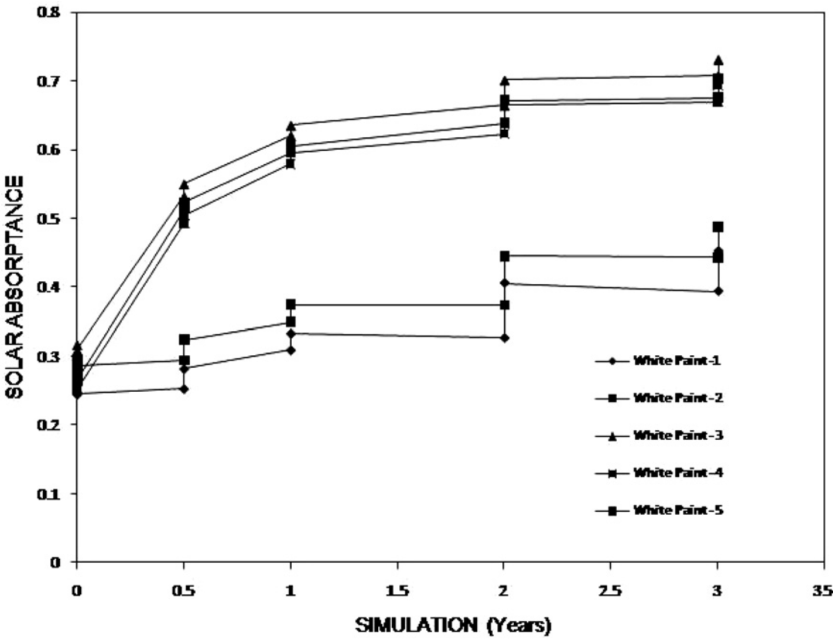

Fig. 11. Solar absorptance degradation of white paints in vacuum during the test.

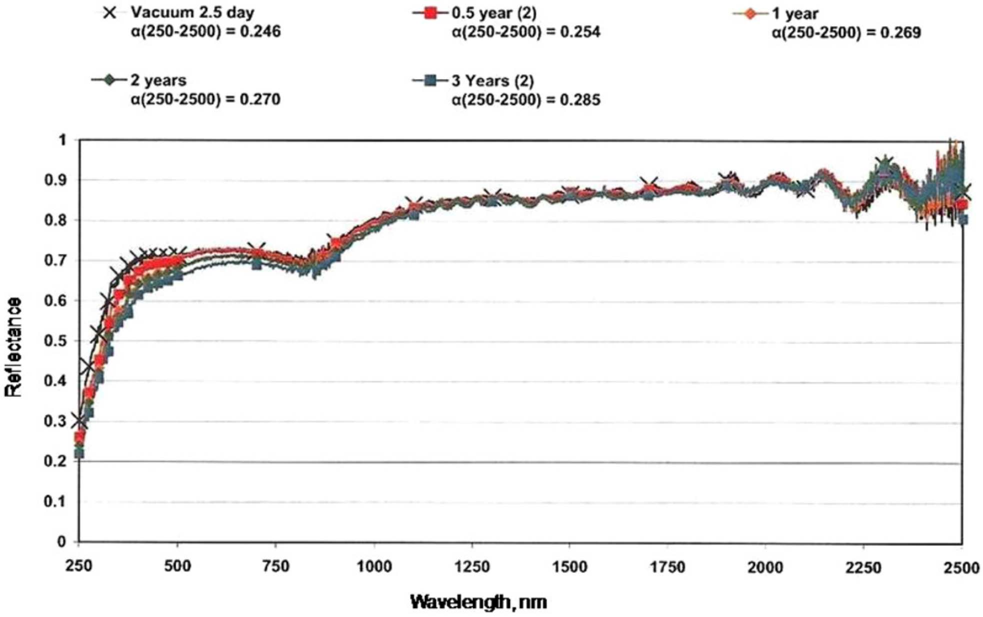

Fig. 12. Reflectance spectrum of white anodized aluminium in vacuum during the test.

The white paints 3, 4, 5 are degraded mainly by UV irradiation. It is an organic binder that degrades in these high gloss paints rather than the pigment. In the more stable paints 1 and 2 having a high diffusing aspect, the binder is silicon based that is more stable under UV (Anvari et al., 2009). The low degradations that are found under particles irradiation are probably due to the stable pigment. The degradation of all the paints during 3 years step is mainly due to particles irradiation as shown in Table 4.

3.8. White anodization

Anodizing is an electrochemical process used for obtaining a protective oxide film on the anodic component. In addition to its protective role, anodic film imparts excellent thermal control properties. The anodic oxide film is a ceramic coating; it has about one-tenth of the thermal conductivity of aluminium and its melting temperature is about 2323 K, far higher than that of aluminium. The infrared emissivity of a polished aluminium sample is only about

0.03, but this can be greatly increased by the anodizing. A 10–15 μm anodic film obtained by conventional sulphuric acid electrolyte provides infrared emissivity of the order of 0.77, whereas its solar absorptance is only around 0.32. The anodic film, therefore, acts as a good solar reflector (Sharma and Bhojaraj, 1989; Sharma et al., 1998; Mukhopadhyay and Sharma, 1997). The optical properties of anodic film can be further improved by suitable modifications in the anodizing process. One of the attractive features of anodic film is the flexibility of its structure and properties. By choosing different pre- and post-anodizing parameters, it is possible to obtain oxide film with different structure, composition and properties. White anodizing provides a solar reflector coating with a low solar absorptance and a high thermal emittance. It is used on the high heat dissipation components to radiate the heat into the outer space.

In the present study, the degradation behavior of white anodizing obtained with double salts of titanium/zirconium, polyhydric alcohol, carboxylic acid and sulphuric acid is investigated (Wernick and Pinner, 1972).

The reflectance spectrum of white anodized sample in vacuum during the test is presented in Fig. 12. The current white anodizing film is found very stable ($\Delta\alpha_S$, +0.039) when compared to that of the process reported earlier ($\Delta\alpha_S$, +0.32) (Marco et al., 2003).

4. Conclusions

A long term radiation test simulating 3 years of a geostationary orbit on North/South faces of a three axes stabilized satellite has been performed. The degradation results of the solar absorptance and emissivity of various thermo-optical materials viz, optical solar reflectors, white anodizing, white paints, black paints, multilayer insulation materials, varnish coated aluminized polyimide, germanium coated polyimide, polyether ether ketone (PEEK) and poly tetra fluoro ethylene (PTFE) are obtained. The effect of the UV and particles irradiations under vacuum and the effect of the transitions between air and vacuum on the degradation of the spectral reflectance and solar absorptance have been evaluated in-situ. Additional measurements have been done ex-situ before and after the irradiations to evaluate the absolute solar absorptance and the emissivity stability. The emissivity changes for all the samples are negligible, at the limits of the measurements uncertainty. The expected good solar absorptance stability of the glass based rigid solar reflectors (UV reflective coated) has been verified. Polymer based flexible reflectors are less stable. Degradation in ITO coated flexible OSR is less when compare to without ITO coating. Moderate degradations of some polymeric samples (aluminized polyimide, ITO coated aluminized polyimide film, varnish coated aluminized polyimide, PEEK and PTFE) is observed, mainly due to the particles irradiation effect, except for the germanium polyimide film, which is highly stable. The white paints are the most degraded. Cracks are visible at the naked eye, on the flexible OSRs and on the varnish coated polyimide. Deeper characterizations of the samples could give more degradation information related to mechanical properties.

Acknowledgements

Authors are thankful to J. Marco and C. Pons of ONERA, France for facilitating the ultraviolet and particulate irradiation tests of our samples.

References

Agarwal, B.N. Design of Geosynchronous Spacecrafts. Prentice Hall, Englewood 273, 281, 1986.

Anvari, F., Farhani, K.S.Niaki Comparative study on space qualified paints used for thermal control of a small satellite. Iranian J. Chem. Eng. 6 (2), 50–62, 2009.

Gilmore, D. G. Spacecraft Thermal Control Handbook, Vol. I: Fundamental Technologies, second ed, The Aerospace Corporation Press, 2002.

Marco, J., Bhojaraj, H., Hulyal, R. Evaluation of thermal control materials degradation in simulated space environment. Proc. 9th Int. Symposium on Materials in Space Environment, Noordwijk, The Netherlands, Compiled by Fletcher, K., June 16–20, 2003 (ESA SP-540, 359–366, September 2003).

Marco, J., Remaury, S., Tonon, C. Eight years GEO ground testing of thermal control coatings. 11th ISMSE, 15-18 Sept., Aixen provence, France, 2009. http://esmat.esa.int/Materials_News/ISME09/pdf/3-Ground/S2-Marco.pdf.

Mukhopadhyay, A.K., Sharma, A.K. Influence of Fe-bearing particles and nature of electrolyte on the hard anodizing behavior of AA-7075 extrusion products. Surf. Coat. Technol. 92, 212–220, 1997.

Sharma, A.K., Bhojaraj, H. Thermoanalytical studies of anodic oxide coatings on aluminium. Plating Surf. Finishing. 76 (2), 59–61, 1989.

Sharma, A.K., Bhojaraj, H., Narayanamurthy, H., Patki, A.V. Hard-anodizing behavior of aluminium alloy DTD5124 containing varying amount of impurities under different electrolytic conditions. Plating Surf. Finishing. 85 (7), 55–59, 1998.

Sharma, A.K. Surface engineering for thermal control of spacecraft. Surf. Eng. 21, 249–253, 2005.

Wernick, S., Pinner, R. Surface Treatment & Finishing of Aluminium and its Alloys. The Teddington, UK, Robert Draper Ltd., fourth ed. Vol. II, p. 545, 1972.